AIP | Review of Scientific Instruments

Picoliter droplets for spinless photoresist deposition

Utkan Demirci

Citation: Review of Scientific Instruments **76**, 065103 (2005); doi: 10.1063/1.1922867
View online: http://dx.doi.org/10.1063/1.1922867
View Table of Contents: http://scitation.aip.org/content/aip/journal/rsi/76/6?ver=pdfcov
Published by the AIP Publishing

Picoliter droplets for spinless photoresist deposition

Utkan Demirci[a)]
E.L. Ginzton Lab., Stanford University, Stanford, California 94305

(Received 24 January 2005; accepted 28 March 2005; published online 17 May 2005)

In this article, we present an acoustically actuated two-dimensional (2D) micromachined ejector array for a zero waste and spinless droplet-by-droplet photoresist deposition method. The theory of operation, the experimental results obtained with acoustic focused 2D micromachined microdroplet ejector array is demonstrated. The ejector operation at 34.7 MHz and generation of 21 μm diam photoresist solvent droplets in drop-on-demand and continuous modes of operation are demonstrated. Photoresist droplets are ejected onto a wafer surface by this acoustic ejector array. Photoresist droplets are ejected on drop on demand and interact with each other by surface tension forces to generate photoresist coverage on the wafer surface during photoresist deposition by droplet generation. By overlapping ejected photoresist droplets, formation of a uniform thickness, line coverage is achieved. Multiple photoresist lines are printed simultaneously by a 3×3 ejector array. By overlapping photoresist lines, coverage of a 4 in. silicon wafer with photoresist is achieved. © *2005 American Institute of Physics*. [DOI: 10.1063/1.1922867]

I. INTRODUCTION

In the fabrication of integrated circuits and microelectromechanical systems (MEMS), deposition of organic polymers by spin coating is the most employed process step.[1] Alternative deposition methods are emerging, such as techniques used in the deposition of doped organic polymers for organic devices [e.g., light emitting diodes (LEDs) and flat panel displays], and deposition of photoresist or dielectric materials for semiconductor manufacturing.[2] Moreover, a reliable and rapid method for dispensing femtoliters to picoliters of fluid has surfaced as a basic need in the fields of biomedicine and biotechnology.[3–7]

Various techniques have been reported for the deposition of organic polymers such as photoresist, and low-*k* or high-*k* dielectrics in semiconductor and MEMS processes.[8] Among the various reported methods for deposition of organic polymers, the spin coating method dominates current industrial applications, since it can fulfill the throughput and quality requirements posed by the integrated circuit industry.[8,9] In spin coating, the coating chemical is poured on top of the wafer, and spun at some speed to properly coat it. This technology relies on centrifugal force and surface tension of the liquid to provide a coating that meets the stringent standard of thickness and uniformity. However, the spin coating technique wastes expensive chemicals, e.g., up to 95% of the photoresist is wasted during spin coating.[9,10] In addition to wasting expensive chemicals, the cost of disposing hazardous waste is high.[10] In order to avoid loss of process yield due to photoresist contamination, the spun-off resist cannot be reused, and must be disposed off carefully. Furthermore, due to the spinning, there is edge bead formation at the edges of the wafer, which has to be removed after the deposition. This causes loss of active area on the wafer and becomes a more important problem as the wafer size increases.[11]

A photoresist deposition method of printing the photoresist onto the wafer drop by drop has the potential to reduce the operational cost associated with the lithograph.[12,13] Photoresist consists of photoactive components and fast-evaporating solvents that makes it very sensitive to heat.[14] This ejection technology relies on the surface tension of the ejected fluid to provide thin film quality and uniform thickness of the deposited photoresist without spinning.[11,13]

There has been previous work in order to form droplet ejection by utilizing an acoustic lens.[15,16] acoustically focused two-dimensional (2D) micromachined microdroplet ejector arrays that we present achieve formation of the focal point by leaky surface acoustic waves. This type of acoustic wave was previously employed by Farnell and Jen in acoustic microscopy.[17] We demonstrate droplet generation by utilizing leaky surface acoustic waves.

We designed and fabricated an acoustically focused 2D micromachined microdroplet ejector array with elements that are individually addressed and controlled for photoresist ejection. Simultaneous photoresist droplet ejection from all the elements of an acoustically focused 3×3 micromachined ejector array is demonstrated. Silicon micromachined microfluid channel spacers are designed and fabricated in order to handle photoresist and other fluid flow during ejection and demonstrated drop-on-demand photoresist ejection, single droplets, and lines printed on the wafer surface and photoresist wafer coverage with the acoustically focused 2D micromachined microdroplet ejector array. Ejection takes place from an open, nozzleless reservoir. The droplet ejection direction does not depend on the nozzle geometry. Furthermore, the device releases acoustic waves at every cycle of actuation, which assures reliability of the acoustic focus formation given that the liquid surface level is stable at the focal

[a)]Currently at: Center for Engineering Medicine, Harvard Medical School, Massachusetts General Hospital, and Shriners Burns Institute; electronic mail: utkan@stanfordalumni.org

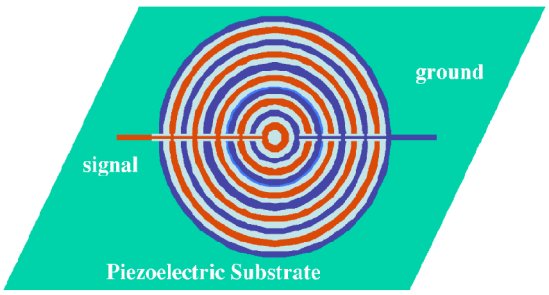

FIG. 1. (Color online). Geometry of the 2D ejector array (top view).

point and thus ensures ejection. The full photoresist coverage of a 4 in. silicon wafer is demonstrated by these ejector arrays without spinning or waste.

II. THEORY

The unit cell of an acoustically actuated microdroplet 2D ejector array is an interdigital ring transducer on a piezoelectric substrate as shown in Fig. 1. This unit cell can be repeated periodically in order to build 2D arrays of ejectors.

A. Radiation pressure analysis

If a fluidic medium is placed on the piezoelectric substrate as shown in Fig. 2, the surface acoustic waves generated by the interdigital ring transducers leak into the medium.[18,19] As the waves travel through the fluid, they form a focus. If the momentum generated by the acoustic radiation pressure overcomes the surface tension forces of the fluid, then a droplet can be ejected as shown in Fig. 2. The free air above the fluid surface has much lower acoustic impedance than that of the ejection fluid. This allows us to assume that the incident wave at the surface is completely reflected back into the fluid. We can assume that the incident and reflected waves will form a wave form at the free boundary of the liquid and air with the following time varying field equations for pressure p_{ac}, density ρ_{ac}, and velocity $\mathbf{v}_{ac}$:[16,18–20]

$$p_{ac} = 2p_{initial}\sin(kz)\cos(\omega t), \tag{1}$$

$$\rho_{ac} = \frac{2p_{initial}\sin(kz)\cos(\omega t)}{c^2}, \tag{2}$$

$$\mathbf{v}_{ac} = \frac{-2p_{initial}\cos(kz)\sin(\omega t)}{c\rho_{bulk}}\hat{z}, \tag{3}$$

where $p_{initial}$ is the pressure amplitude of the incident acoustic wave, ρ_{bulk} is the bulk density of the liquid, c is the velocity, $\omega = 2\pi f$ is the angular velocity, and $k = \omega/c$ is the wave number of the acoustic wave in the liquid. The subscript ac indicates the varying fields at the frequency f.

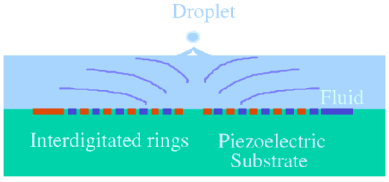

FIG. 2. (Color online). Physical operation of a fluid loaded 2D ejector array (side view).

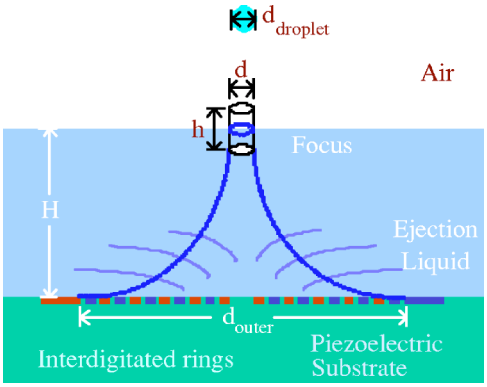

FIG. 3. (Color online). The cylindrical acoustic focus at the surface of the fluid.

Chu and Apfel[20] give the Langevin radiation pressure $\aleph$ by the mean energy density U of the acoustic beam at the surface of the air liquid boundary $(z=0)$[21]

$$U(z=0) = \frac{1}{T_0}\int_0^{T_0}\frac{1}{2}\left(\rho_{bulk}v_{ac}^2 + \frac{p_{ac}^2}{c^2\rho_{bulk}}\right)dt = \frac{p_{initial}^2}{c^2\rho_{bulk}}, \tag{4}$$

The time averaged energy density is computed by Eq. (4).[19–21] Hunter gives the average intensity of the incident wave $I_{initial}$ as in Eq. (5) and the Langevin radiation pressure $\aleph$ as in Eq. (6).

$$I_{initial} = \frac{p_{initial}^2}{2c\rho_{bulk}}, \tag{5}$$

$$\aleph = \frac{2I_{initial}}{c}. \tag{6}$$

The radiation pressure acts for a time of T, which generates an initial momentum of $\Psi_{initial}$ per unit area

$$\Psi_{initial} = \aleph T. \tag{7}$$

We assume that the initial momentum is given to a cylinder of ejection fluid and is uniformly distributed in that cylinder such that the full width at half maximum of the acoustic focus is at the midpoint of the focal fluid cylinder as shown in Fig. 3.

The diffraction limited acoustic beam expressions are given by the following equations:[19]

$$d = 1.02\lambda F$$

and

$$h = 7.1\lambda F^2, \tag{8}$$

where F is the focal number (F number) of an equivalent acoustic lens. The F number is given by the ratio of the focal length to the aperture of a lens. Here, we develop a simple formulation for the F number of the devices using this definition through Eqs. (9)–(11).

The speed of the surface acoustic wave in the piezoelectric substrate v_{piezo} is larger than the speed of the acoustic wave in water v_{water}. The circular converging leaky Rayleigh waves propagate into the fluid at an angle of Φ, which is given by the following equation:

$$\Phi = \arcsin\left(\frac{v_{\text{water}}}{v_{\text{piezo}}}\right). \tag{9}$$

The location of the focal point H can be calculated from this angle and the outer diameter of the device d_{outer}

$$H = \frac{d_{\text{outer}}}{2}\tan\Phi = \frac{d_{\text{outer}}}{2}\tan\left[\arcsin\left(\frac{v_{\text{water}}}{v_{\text{piezo}}}\right)\right]. \tag{10}$$

The F number then can be calculated as in the following equation:

$$F = \frac{H}{d_{\text{outer}}} = \frac{\frac{d_{\text{outer}}}{2}\tan\Phi}{d_{\text{outer}}} = \frac{1}{2}\tan\left[\arcsin\left(\frac{v_{\text{water}}}{v_{\text{piezo}}}\right)\right]. \tag{11}$$

The energy E in the incident burst is given by Eq. (12), and all energy values represent the total energy of the acoustic pulse at the focal plane[16]

$$E = I_{\text{initial}}AT. \tag{12}$$

The initial momentum applied to the bottom area of the cylinder is given by the following equation:

$$P_{\text{initial}} = \Psi_{\text{initial}}A = \aleph TA = \frac{2I_{\text{initial}}AT}{c} = \frac{2E}{c}. \tag{13}$$

We can assume as a simple model that this initial momentum is transferred to the fluid cylinder mass being ejected as a droplet with a velocity. The volume of the cylinder of fluid V_{cylinder} that lies under the focal plane is given by Eq. (14) and the mass of the droplet m_{droplet} is given in Eq. (15). This momentum transfer results in the initial droplet velocity of the droplet v_{initial} as shown in Eqs. (16) and (17). The initial velocity is expected to increase with the initial input energy. The increase in the initial droplet velocity with the frequency can be simply understood by smaller droplet sizes as the frequency increases, if a constant momentum input is assumed as can be seen from Eqs. (16) and (17).

$$V_{\text{cylinder}} = \pi\left(\frac{h}{2}\right)\left(\frac{d}{2}\right)^2, \tag{14}$$

$$m_{\text{droplet}} = \rho_{\text{bulk}}V_{\text{cylinder}} = \rho_{\text{bulk}}\pi\left(\frac{h}{2}\right)\left(\frac{d}{2}\right)^2, \tag{15}$$

$$P_{\text{initial}} = m_{\text{droplet}}v_{\text{initial}}, \tag{16}$$

$$v_{\text{initial}} = \frac{P_{\text{initial}}}{m_{\text{droplet}}}\alpha E f^3. \tag{17}$$

The ejected droplet diameter may be projected by equating the V_{cylinder} to the volume of a spherical droplet V_{cylinder} of diameter d_{droplet} as shown in the following equations:

$$V_{\text{cylinder}} = \pi\left(\frac{h}{2}\right)\left(\frac{d}{2}\right)^2 = V_{\text{droplet}} = \frac{4}{3}\pi\left(\frac{d_{\text{droplet}}}{2}\right)^3, \tag{18}$$

$$d_{\text{droplet}} = \sqrt[3]{\frac{3}{4}hd^2\alpha}\left(\frac{1}{f}\right). \tag{19}$$

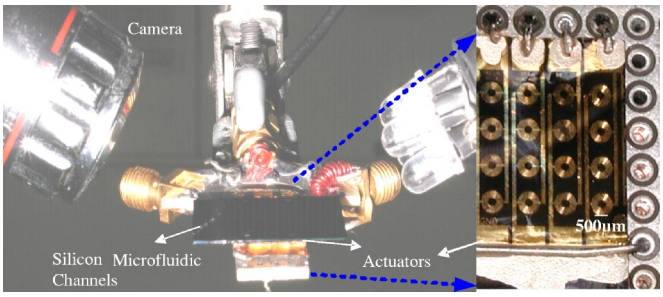

FIG. 4. (Color online). The spacer aligned on top of the 4×4 ejector array with silicon micromachined microfluidics channels that control fluid level.

III. METHODS AND RESULTS

The picture of the fabricated 4×4 ejector array is shown in Fig. 4. Each 1×4 row of the 2D array is individually addressed as can be seen from the picture of the device. In order to achieve droplet ejection not only in an upward direction but in all directions (sideways, downward), and control the focus location without being effected by the evaporation or the tilt of the device, the silicon microfluidic channel spacers were designed so that the fluid could continuously fill the spacer ejection openings through the fluidic channels, keeping the fluid level constant.

The input signal to the ring ejector array is a tone burst. The burst repetition rate determines the drop ejection rate. The ring array ejected various fluids such as photoresist, water, and solvents (acetone, isopropanol, methanol, and ethanol), at a drop ejection rate of 1 kHz–0.1 MHz. Figure 5 shows 21 μm diam photoresist solvent droplets ejected upward into the air at 1 kHz with a 7 μs long tone burst at 34.7 MHz.

A. Droplet ejection and imaging

Stroboscopic imaging techniques were used to view the ejected droplets. The jet of droplets could be viewed by a

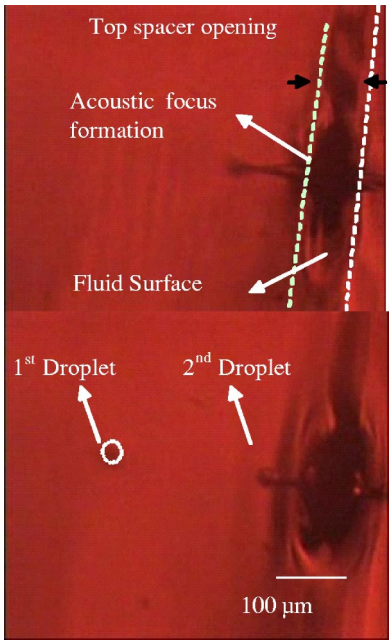

FIG. 5. (Color online). Ejected 21 μm diam photoresist solvent droplets from a 100 μm wide spacer opening.

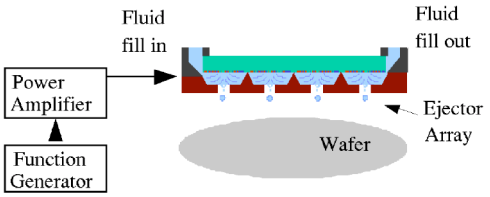

FIG. 6. (Color online). Block diagram of the photoresist deposition setup.

liquid crystal display camera (Sony, SSC-CD33V, Japan) with a microscopic lens [10×, numerical aperture (NA) 0.13, Olympus, Japan]. The downward ejection of photoresist solvent droplets through a 100 μm wide fluid spacer opening is shown in Fig. 5. The ejection of a single droplet followed by an evolving second droplet through a neck of acoustically raised fluid focus can be seen in Fig. 5.

B. Photoresist coverage experiments

The experiments with photoresist are demonstrated. We first ejected single droplets of photoresist (Shipley 3612) on drop on demand onto a silicon wafer. We continued our experiments by overlapping many droplets laterally, which resulted in photoresist lines. Finally by repeating these lines separately side by side or by printing many lines simultaneously we covered wafer surfaces with photoresist.

Photoresist droplets are ejected onto a wafer surface by an acoustically actuated micromachined 2D ejector array. A spinless setup for photoresist coverage experiments is shown in Fig. 6. The wafer was placed on a micrometer stage which enables us to eject photoresist droplets at the desired locations in the wafer surface by drop-on-demand capability.

Photographs of the ejected photoresist droplets on the wafer were taken through a microscope (Eclipse ME600, Nikon Corp., Japan, 10× magnifications, NA 0.3). The droplet profile data such as the step heights and roughness of the photoresist surface of the ejected droplets were collected by a Dektak IIA (Veeco Instruments Inc., Woodbury, N.Y.) profilometer with a 0.1 μm vertical resolution. Dektak IIA utilized a 12.5 μm radius stylus with a wedge angle of 10° in contact with the wafer surface and then translated it along the surface of the substrate with a speed of 0.2 mm/s.

C. Line formation: simultaneous ejection from a micromachined 2D ejector array

Shipley 3612 photoresist was ejected at varying frequencies from 0.1 to 10 kHz. The wafer was moved fast enough under the ejector so that the single photoresist droplets could land on the wafer surface at desired locations. By changing the frequency of ejection or decreasing the speed of the wafer movement, the location where the droplets land can be exactly determined and a line can be formed from single droplets overlapping each other.

Simultaneous ejection from two array elements resulted in two lines written in parallel to each other. The separation lateral angle of the 2D ejector array with respect to the direction of the movement of the micrometer stage can be controlled such that the separation between the simultaneously ejected lines can be determined. Figure 7(a) demonstrates two simultaneously written lines that do not overlap. Figure 7(b) demonstrates two simultaneously printed overlapping lines. When the lines overlap, it is possible to write wider or thicker photoresist lines depending on the actuation preference. The profiles of a single photoresist droplet, a 40 mm long single photoresist line, and a wider photoresist line obtained by overlapping two simultaneously ejected photoresist lines by 150 μm are shown in Fig. 8.

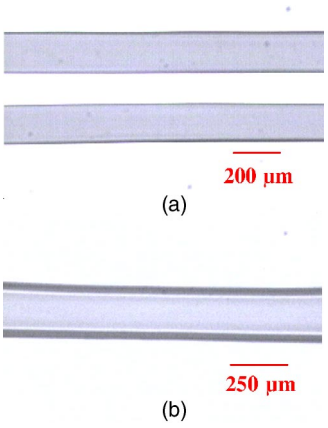

FIG. 7. (Color online). Two simultaneously written photoresist lines on wafer surface; (a) separated and (b) overlapping by 150 μm in order to write a wider 250 μm wide line.

D. Coverage of a wafer surface with photoresist

It was demonstrated that two lines can be overlapped to form a wider line. Next, we demonstrate that the photoresist lines can be repeated side by side such that we can fully coat a silicon wafer with photoresist as shown in Fig. 9. The coverage experiments were conducted in a dry laboratory environment. The thickness of the photoresist film can be decreased by decreasing the number of droplets per location or by decreasing the overlap between two photoresist lines drawn side by side.

A spinless photoresist coating of a 4 in. wafer is shown in Fig. 9. The picture is taken when 2/3 of the wafer area is

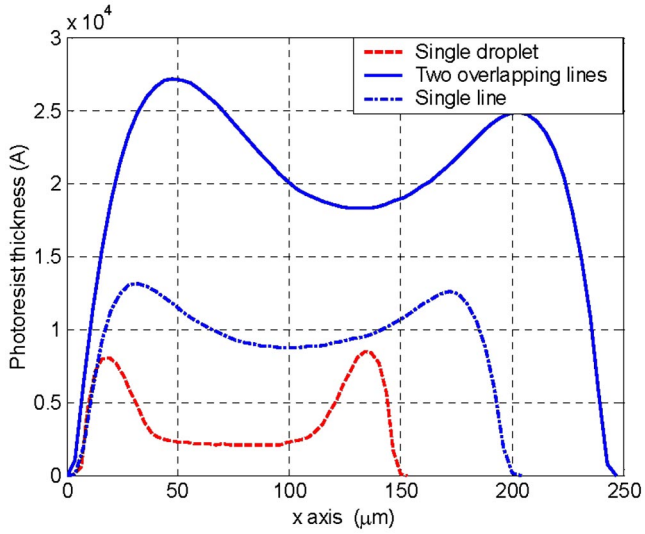

FIG. 8. (Color online). Photoresist single drop, single line, and two overlapping line profiles on the wafer surface of two simultaneously ejected overlapping lines.

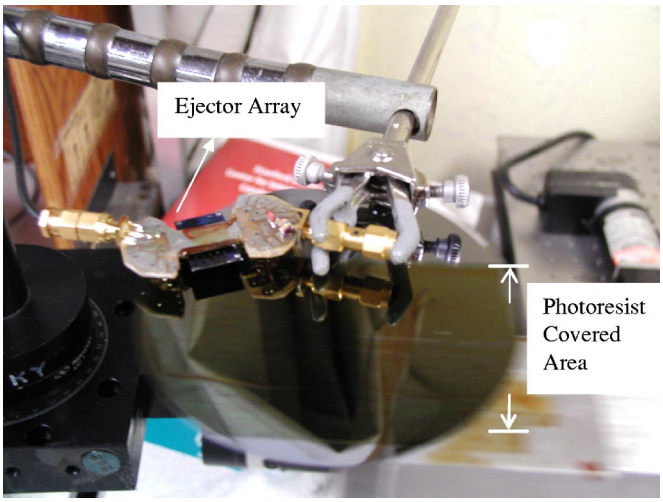

FIG. 9. (Color online). Full photoresist coverage of a 4 in. wafer with 2.4 μm thick photoresist.

covered. The photoresist covered areas are dark and can be distinguished from the shiny silicon wafer surface. During coverage, the wafer is moved at a speed of 2 cm/s as the photoresist ejection is performed at 1 kHz. This corresponds to one droplet per 20 μm separation for the formation of a single line. Photoresist lines were written in parallel to perform the full coverage. The separation between two lines was set to 140 μm. The separation between droplets and lines can be modified, which eventually determines the overall photoresist thickness. The photoresist thin film thickness was measured to be 2.4 μm and thickness uniformity was measured to vary by ± 0.02 μm at the most uniform coated areas of the wafer and ± 0.3 μm at the areas with the worst uniformity. The surface roughness was measured to vary from 68 to 600 A over the wafer. There was no spinning involved in the process and the coverage experiments were done in a dry laboratory environment.

IV. DISCUSSION

In the experimental full wafer coverage work, the lines were drawn at a speed of 2 cm/s, at 1 kHz ejection rate. A single pass over a 4 in. wafer would take $4 \times 2.54/2 = 5.1$ s at this speed and ejection rate during the drawing of a photoresist line over the diameter. Covering a 4 in. wafer by a single ejector by overlapping parallel lines assuming for simplicity that all are the same length as the diameter and by setting the separation between two lines to 140 μm would take $4 \times 2.54/0.014 = 725$ passes. Therefore, the time it would take to cover a 4 in. wafer by a single ejector ejecting is $725 \times 5.1/60 = 61$ min. Although this coverage time is long, it should be signified that this is for coating a whole wafer with a single ejector. The potential for the time it would take to cover a wafer by using an array of ejectors can be as small as a few seconds. One could imagine hundreds of these ejectors placed side by side in a linear array or 2D array format, printing a single line wide enough to cover a whole wafer by a single pass over the wafer. The wafer movement speed can be easily increased. The ejection rate could also be easily raised to 10 kHz. This demonstrates a potential to decrease the whole wafer coverage down to 0.5 s given that there are no other problems due to wafer speed. This would remarkably increase the throughput of coating. The potential for increase in the throughput is clearer, when we consider that there is no spinning or edge bead removal processes necessary after the coating step, which takes about 1 min to complete in today's commercial track systems by using the spin coating method.

The future of micromachined ejectors is full of possibilities for innovation. There is room for increasing the uniformity of the deposited thin films and decreasing the throughput of coverage by increasing the number of ejector elements of the 2D ejector array that ejects simultaneously for this specific semiconductor photoresist coating application. The direct printing capabilities for semiconductor applications stand as very interesting avenues to be explored. Moreover, other possible applications in various fields of research such as drug testing and delivery in biotechnology predict a bright future for the micromachined acoustically actuated 2D microdroplet fluid ejectors.

[1] L. M. Peurrung and D. B. Graves, IEEE Trans. Semiconductor Manufacturing **6**, 72 (1993).
[2] T. R. Hebner, C. C. Wu, D. Marcy, M. H. Lu, and J. C. Strum, Appl. Phys. Lett. **72**, 519 (1998).
[3] C. M. Roth and M. L. Yarmush, Ann. Rev. Biomed. Eng. **1**, 265 (1999).
[4] J. M. Jaklevic, H. R. Garner, and G. A. Miller, Ann. Rev. Biomed. Eng. **1**, 265 (1999).
[5] P. Luginbuhl *et al.*, Proceedings Transducers 1999, pp. 1130–1133.
[6] A. V. Lemmo, J. T. Fisher, H. M. Geysen, and D. J. Rose, Anal. Chem. **69**, 543 (1997).
[7] A. V. Lemmo, D. J. Rose, and T. C. Tisone, Curr. Opin. Biotechnol. **9**, 615 (1998).
[8] B. Bednar, J. Kralicek, and J. Zachoval (Elsevier Science B.V., Amsterdam, 1993), pp. 77–82.
[9] J. Derksen, S. Han, and J.-H. Chun, Semiconductor Manufacturing Conference Proceedings, IEEE International Symposium, 11–13 October 1999, pp. 245–248.
[10] G. Percin and B. T. Khuri-Yakub, 16, 452 (2003).
[11] G. Percin, dissertation, Stanford University, 2002, Chaps. 1 and 6.
[12] U. Demirci, G. Yaralioglu, E. Hæggström, G. Percin, S. Ergun, and B. T. Khuri-Yakub, IEEE Trans. Semicondutor Manufacturing 517 (2004).
[13] U. Demirci, G. Yaralioglu, E. Hæggström, and B. T. Khuri-Yakub, IEEE Trans. Semiconductor Manuf. (accepted).
[14] J. D. Plummer, M. D. Deal, and P. B. Griffin, *Silicon VLSI Technology—Fundamentals, Practice and Models* (Prentice Hall, Englewood Cliffs, N.J., 1999).
[15] B. Hadimioglu, S. Elrod, and R. Sprague, Proc.-IEEE Ultrason. Symp. 627 (2001).
[16] S. A. Elrod, B. Hadimlioglu, B. T. Khuri-Yakub, E. G. Rawson, E. Richley, C. F. Quate, N. N. Mansour, and T. S. Lundgren, J. Appl. Phys. **65**, 3441 (1989).
[17] G. W. Farnell and C. K. Jen, Electron. Lett. **16**, 541 (1980).
[18] B. A. Auld, *Acoustic Fields and Waves in Solids* (Krieger, Malabar, Fla.).
[19] G. S. Kino, *Acoustic Waves: Devices, Imaging, and Analog Signal Processing* (Prentice Hall, Englewood Cliffs, N.J.).
[20] B. Chu and R. E. Apfel, J. Acoust. Soc. Am. **72** (1982).
[21] J. L. Hunter, *Acoustics* (Prentice Hall, Englewood Cliffs, N.J., 1957).